[redacted]

NACA

RESEARCH MEMORANDUM

AIRPLANE CONFIGURATIONS FOR CRUISE AT A MACH NUMBER OF 3

By Donald D. Baals, Thomas A. Toll, and Owen G. Morris

Langley Aeronautical Laboratory
Langley Field, Va.

CLASSIFIED DOCUMENT

NATIONAL ADVISORY COMMITTEE
FOR AERONAUTICS

WASHINGTON

August 4, 1958

[redacted]

NATIONAL ADVISORY COMMITTEE FOR AERONAUTICS

RESEARCH MEMORANDUM

AIRPLANE CONFIGURATIONS FOR CRUISE AT A MACH NUMBER OF 3*

By Donald D. Baals, Thomas A. Toll, and Owen G. Morris

SUMMARY

Relative to the problem of efficient cruise at a Mach number of 3, wind-tunnel tests have been made of four complete configurations based on widely different aerodynamic approaches and giving promise of high lift-drag ratios. These designs included a highly cambered arrow-wing configuration with 75° of sweep, a 70° swept-wing configuration with control surfaces on booms outboard of the wing tips, a canard configuration with a low-aspect-ratio clipped delta wing employing tip ventrals, and a delta-wing configuration having an aspect ratio of 3. These model designs met, in most cases, minimum requirements of volume, engine simulation, stability, and trim applicable to a long-range bomber design. The design concepts and results, however, are believed to be generally applicable.

Although the experimental programs were not sufficiently complete for an evaluation of the special features, high lift-drag ratios were obtained in all cases. Maximum lift-drag ratios of about 6 were measured at a Mach number of 3 for conditions of fixed transition at test Reynolds numbers of 2 to 4 million. These values extrapolate to maximum lift-drag ratios on the order of 7.5 for full-scale Reynolds numbers of about 100 million. The various configurations differed appreciably in minimum drag and in drag due to lift. There is reason to believe that significant performance improvements can still be achieved, perhaps by combining some of the more attractive features of the different configurations.

INTRODUCTION

The problem of efficient cruise at a Mach number of 3 has placed great emphasis on the achievement of high lift-drag ratios. Relative to this problem, certain aerodynamic approaches appear to have merit. These approaches include optimumizing the total lift distribution for minimum induced drag, the development of favorable lift interference, and the decrease of minimum drag through component design.

*Title, Unclassified.

For the most part, experimental support at a Mach number of 3 for these approaches has been limited to rather elementary models; that is, studies involving wing-body combinations or single components. During the last year the National Advisory Committee for Aeronautics has made experimental studies wherein essentially complete configurations incorporating some of the more promising ideas were investigated in the Mach number range near 3.

Results of four of these model studies are presented. To provide a valid basis for comparison, these model designs usually met minimum requirements of volume, engine simulation, stability, and trim. In general, these configurations were laid out to meet requirements for a long-range-bomber design; however, the design concepts and results should be generally applicable. All test results were obtained under conditions of transition fixed near the leading edges of all surfaces. Inlet air flow was provided for all models, and a drag correction was made for the measured internal momentum losses.

It should be noted that the configurations presented in the present study are not regarded as optimum, and comparative results should not be considered indicative of the ultimate potential of each approach.

SYMBOLS

The lift, drag, and pitching-moment results are given with respect to the wind-axes system; whereas, lateral stability results correspond to body axes. All of the basic moment data are nondimensionalized in terms of wing areas, wing spans, and assumed center-of-gravity locations as given for the various models in the following table.

Model	Wing area, S, sq ft	Wing span, b, ft	Wing mean aerodynamic chord, $\bar{c}$, ft	Center-of-gravity location	
				Distance from nose, ft	Fraction $\bar{c}$
Arrow-wing	3.49	2.50	1.70	2.33	----
Outboard-tail	1.74	2.00	1.08	2.37	0.65
Canard	4.18	1.94	2.25	3.36	.24
Delta-wing	.13	.625	.277	.277	.50

[redacted]

The coefficients and symbols are defined as follows:

C_L	lift coefficient, $\frac{\text{Lift}}{qS}$
$C_{L,OPT}$	lift coefficient at maximum $\frac{L}{D}$
C_D	drag coefficient, $\frac{\text{Drag}}{qS}$
$C_{D,MIN}$	minimum drag coefficient
$C_{D,0}$	zero-lift drag coefficient
$C_{D,0}'$	nominal zero-lift drag coefficient
C_m	pitching-moment coefficient, $\frac{\text{Pitching moment}}{qS\bar{c}}$
$C_{m,0}$	zero-lift pitching-moment coefficient
C_f	skin-friction coefficient
$\frac{L}{D}$	lift-drag ratio
$\left(\frac{L}{D}\right)_{MAX}$	maximum lift-drag ratio
q	dynamic pressure, lb/sq ft
S	wing area, sq ft
A	wing aspect ratio, $\frac{b^2}{S}$
λ	wing taper ratio, $\frac{\text{Tip chord}}{\text{Root chord}}$
Λ	leading-edge sweep angle, deg
b	wing span, ft
$\bar{c}$	wing mean aerodynamic chord, ft

[redacted]

$\frac{t}{c}$	ratio of section thickness to section chord
$\left(\frac{t}{c}\right)_r$	ratio of wing-root thickness to wing-root chord
R	Reynolds number based on $\bar{c}$
M	Mach number
δ_h	incidence of wing-tip horizontal trimming surface, relative to adjacent wing chord line, deg
δ_c	incidence of canard trimming surface, deg
α	angle of attack, deg
C_{n_β}	directional stability derivative
C_{l_β}	effective dihedral derivative
$\frac{\partial C_D}{\partial C_L{}^2}$	drag-due-to-lift parameter
$\frac{\partial C_m}{\partial C_L}$	longitudinal stability parameter

PRESENTATION OF RESULTS

The Arrow-Wing Model

Figure 1 shows the configuration characteristics of the arrow-wing model. This model is an application of the arrow-wing approach to the problem of obtaining a high lift-drag ratio. This approach is discussed in reference 1. For the complete configuration presented herein, the wing leading edge has a 75° angle of sweep. A minimum fuselage is employed with the main volume in the wing. Engine simulation is provided by six separate nacelles, each alined with the local streamlines for minimum drag. All moving control surfaces are located at the wing tips in order to provide longitudinal and directional stability and control.

The wing was designed on the basis of linear theory by using an optimum combination of four loads based on an adaptation of methods presented in references 2 and 3. The wing plan form and idealized

[redacted]

loading distribution were modified in the region of the wing tip in an attempt to reduce the local lift coefficients. The foregoing analytical procedures provided theoretical values for the drag due to lift and the lift-curve slope. The zero-lift wave drag for the complete configuration was estimated from linear theory as the sum of the individual drag of the various components without correction for interference effects. To this value was added the theoretical skin-friction drag (ref. 4) for a turbulent boundary layer at test Mach number and Reynolds number conditions for evaluation of the minimum drag.

Figure 2 shows the basic longitudinal characteristics of the arrow-wing model at $M = 2.87$ for two control deflections (ref. 5). The computed linear-theory values are also shown. The minimum drag coefficient of 0.0110 agrees well with the estimate, but the experimental drag due to lift is considerably higher than calculated. This high drag due to lift caused the $\left(\frac{L}{D}\right)_{MAX}$ to fall considerably below the estimate, but the value of 6.2 obtained is still relatively high.

The arrow-wing model has a positive value of $C_{m,0}$ due to the "washout" at the wing tips, and the configuration trims at $\left(\frac{L}{D}\right)_{MAX}$ with a very small control deflection. The pitching-moment curves are fairly linear up to the test limit of about $0.2C_L$, although it appears that some reduction in stability has begun at that point.

Outboard-Tail Model

The configuration of figure 3 is referred to as the outboard-tail model. The underlying aerodynamic approach resembles, in some respects, that of the previous arrow-wing design. The lifting surfaces are contained essentially within the Mach cone from the wing apex, with the lifting outboard tails providing variation in spanwise as well as longitudinal loading distributions. Favorable drag due to lift is expected to result from the upwash field at the horizontal tails, which allows them to carry an upload at negative tail incidence. Similarly, the sidewash field at the vertical tails can be utilized to provide some additional drag reduction.

This particular arrangement of components was influenced by research directed at obtaining favorable lift characteristics in take-off and landing as well as acceptable stability characteristics through the speed range. A detailed discussion of the design concept is given in reference 6. Engine simulation is provided by a "three-over-three" engine pack exhausting at the fuselage base.

[redacted]

Figure 4 shows the longitudinal characteristics of the outboard-tail configuration at $M = 2.97$ for two control deflections. All coefficients and the given aspect ratio are based on wing plus horizontal-tail area and on the total span. The results presented were obtained as a part of the investigation reported in reference 7.

The maximum lift-drag ratio is about 5.85, with a minimum drag coefficient of about 0.0150. This high value of minimum drag results in part from the fact that this model has approximately double the specified minimum volume. The agreement of experiment with the estimated characteristics is shown to be reasonably good up to maximum $\frac{L}{D}$ but only fair at higher lifts.

In estimating the model lift, only the wing and the horizontal tails were considered. For each of these components, the linear-theory lift slope of the isolated surface was calculated. Also, a calculation of the wing-generated flow field at the tails indicated a rate of change of effective upwash angle with angle of attack of 0.7. This interference effect along with the characteristics of the isolated surfaces yielded the lift estimate shown for the model. Drag due to lift was assumed to be determined by the reciprocal of the lift-curve slope of the wing and of the horizontal tail, with appropriate consideration again given to the vector components of the upwash field. Zero-lift drag was obtained by simple addition of the wave and skin-friction contributions of the components, as in the case of the arrow-wing model.

The outboard-tail model has a positive value of $C_{m,0}$ caused by 3° of washout at the wing tip, and this model trims at $\left(\frac{L}{D}\right)_{MAX}$ for essentially zero control deflection. In its present form, however, this configuration at $M = 2.97$ becomes longitudinally unstable somewhat above the cruise lift coefficient. Subsonic tests, however, indicate that no serious problem exists through the range of take-off lift coefficients. A modified configuration with 60° sweep has been developed in an attempt to alleviate this supersonic stability problem.

Canard Model

Figure 5 shows the configuration characteristics of the canard model. The engine-wing combination is designed to optimumize interference lift at $M = 3$ by positioning the shock from the inlet wedge just behind the leading edge of the wing lower surface. Wing-tip fins are used to reflect these shocks for a further lift increment and to provide directional stability at angles of attack. On the upper surface of the wing the location of the wing ridge line and the shape of the fuselage afterbody have been selected to improve lift-drag interference.

[redacted]

Canard controls along with a modified elliptical fuselage having a nose cant of about 3° have been incorporated in order to achieve efficient trim characteristics.

Figure 6 presents the basic longitudinal characteristics plotted against lift coefficient at M = 3. These results were obtained for a configuration revised from the preliminary model reported in reference 8. The revision consisted of the upward nose cant and addition of upper-surface area to the wing tip fins. The maximum value of lift-drag ratio for the canard configuration is about 6.0, and the minimum drag coefficient is about 0.0120. The configuration is trimmed at maximum $\frac{L}{D}$ with a very small canard deflection but with a low stability margin. Note that the pitching-moment curves are essentially linear over the test lift-coefficient range.

The evident correlation with the estimated characteristics, shown as dashed curves, is an indication that the configuration is performing as anticipated. The estimates are admittedly approximate, however. The configuration lift was estimated as the sum of the isolated canard lift plus the lift of the wing assumed to be a full delta wing in an attempt to approximate the effect of the tip fins. A linear-theory calculation of the interference lift and drag of an undersurface wedge which simulated the solid volume of the engine pack was also included in the estimate. Drag due to lift was assumed equal to the reciprocal of the lift-curve slope, while the zero-lift drag was obtained by simple addition of the component contributions of wave and skin-friction drag.

Delta-Wing Model

Figure 7 shows the configuration characteristics of a delta-wing model having a leading-edge sweep of 53°. The configuration chosen was the result of a systematic study made of a family of wings in the Langley 9-inch supersonic tunnel, the initial phases of which are reported in reference 9. The 2-percent-thick wing is of relatively high aspect ratio, and its leading edge is supersonic at M = 3. This configuration was designed to obtain high lift-drag ratios by a simple combination of low-drag elements. A small $\frac{2}{3}$-power body was located on the underside of the wing with engine simulation provided by six separate internal-compression nacelles.

It should be noted that this configuration is not strictly comparable to the previous models. It has only about one-third the equivalent internal volume of the canard and arrow-wing models, and no control surfaces are provided for trim. The rather large base area has been corrected to free-stream static-pressure conditions.

[redacted]

Figure 8 presents the longitudinal characteristics at $M = 2.91$. The maximum lift-drag ratio for the untrimmed delta-wing configuration is about 6.3, with a minimum drag coefficient of 0.0094 which is the lowest of all configurations tested. The experimental agreement with the theoretical estimates for the delta-wing model is very good. The lift-curve slope was assumed equal to the linear-theory value of $\frac{4}{\sqrt{M^2 - 1}}$, which is applicable to delta wings with supersonic leading edges. Drag due to lift was assumed equal to the reciprocal of the lift-curve slope, while the zero-lift drag was estimated by methods similar to those for the previous models.

Lateral Characteristics

Lateral characteristics of the four models that have already been discussed are summarized in figure 9. This figure shows the directional stability derivative C_{n_β} and the effective dihedral derivative C_{l_β} plotted against angle of attack for the test Mach number nearest 3.0. Note that all models are directionally stable at the test angles of attack. The arrow-wing, outboard-tail, and canard models have fairly substantial values to angles of attack of at least 10°; whereas, at the single test condition of 0° angle of attack, the delta-wing model was marginally stable. The derivative C_{l_β} ranged from essentially zero in the cruise range for the outboard-tail model to fairly large positive effective dihedral (negative C_{l_β}) for the arrow wing. No results were obtained for the delta-wing model.

ANALYSIS OF RESULTS

Variation of $\left(\frac{L}{D}\right)_{MAX}$ With Mach Number

Figure 10 presents the variation of experimental maximum lift-drag ratio with Mach number for the four basic configurations. In general, $\left(\frac{L}{D}\right)_{MAX}$ decreases with increasing Mach number, as would be expected from the theoretical increase in drag due to lift.

The most rapid decrease in $\left(\frac{L}{D}\right)_{MAX}$ with Mach number occurs for the arrow-wing configuration. This rapid decrease near $M = 3$ is believed to result from a combination of insufficient sweep and the use of airfoil sections having excessive thickness. This combination leads to

local transonic shocks and attendant flow separation. The arrow-wing configuration accordingly exhibits much more favorable $\frac{L}{D}$ characteristics at the lower test Mach number.

The canard configuration, on the other hand, shows a marked peak in $\left(\frac{L}{D}\right)_{MAX}$ at $M = 3$. This might be expected, since the inlet-wing combination was designed for peak efficiency at this Mach number. Supplementary data, wherein the Mach number and angle of leading-edge sweep were varied, show that the peak may occur rather abruptly near $M = 3$. It should be noted that although the canard configuration has a relatively low aspect ratio of 0.9, the values of $\frac{L}{D}$ obtained are comparable to those obtained by the other configurations which had much higher aspect ratios.

It will be noted that at Mach numbers near 3, all configurations have a maximum lift-drag ratio of about 6. This fact is more of a coincidence than a general conclusion, for the lift-drag ratios are shown later to result from widely differing characteristics.

Drag Polar Analysis

In order to achieve a better understanding of the lift-drag ratio trends, it is necessary to study the elements that contribute to the form of the drag polar. Figure 11 shows the method that has been adopted in this study. The objective is to divide the total drag into a drag coefficient at zero lift and a drag-due-to-lift term. The experimental drag data are plotted against C_L^2. As is generally true with wings having camber, twist, or some means for obtaining favorable lift interference, C_D does not vary linearly with C_L^2. Therefore, in a strict sense the drag due to lift cannot be defined precisely by a single term proportional to C_L^2.

For practical purposes, however, a single-term method can be devised to represent the most significant portion of the drag polar by drawing a straight line tangent to the experimental curve of C_D plotted against C_L^2 at the point corresponding to $\left(\frac{L}{D}\right)_{MAX}$. The slope of the tangent gives the value of $\frac{\partial C_D}{\partial C_L^2}$, and the intercept at zero lift is a nominal drag value of $C_{D,0}$ usually slightly less than the experimental minimum drag but close to the minimum drag that would be measured for a

symmetrical model with the twist and camber removed. With the parameters $\frac{\partial C_D}{\partial C_L^2}$ and $C_{D,0}'$ determined, the effects of independent variation of these parameters on $\left(\frac{L}{D}\right)_{MAX}$ and on the optimum lift coefficient can be studied through simple equations such as those shown in figure 11. These equations form the basis for estimating the effects of Reynolds number on $\frac{L}{D}$ and $C_{L,OPT}$ presented later. For the subsequent analysis, values of $C_{D,0}'$ are not presented, but data are given for $C_{D,MIN}$ which, for the configurations considered, is generally only slightly greater than $C_{D,0}'$.

Variation of $C_{D,MIN}$ and $\frac{\partial C_D}{\partial C_L^2}$ With M

Figure 12 shows the variation in $C_{D,MIN}$ and $\frac{\partial C_D}{\partial C_L^2}$ with Mach number for the four basic configurations. Relative to the minimum drag at M = 3, it will be noted that there is about a 50-percent variation in $C_{D,MIN}$, from the low value for the delta-wing model to the high value for the outboard-tail model. This difference is caused, in part, by the greatly differing levels of internal volume. The delta-wing model has about one-third the volume of the arrow-wing and canard models, while the outboard-tail model has about twice their volume.

Relative to the minimum drag of these configurations, the skin friction at test Reynolds numbers is the major component and ranges from about $1\frac{1}{2}$ to 3 times the value of the estimated pressure drag. These values indicate the great importance of testing under known boundary-layer conditions, for any variation in skin friction can completely mask the pressure drag.

The drag-due-to-lift characteristics are also shown in figure 12. In all cases the drag due to lift increases with increasing Mach number as predicted by linear theory. The outboard-tail configuration is shown to have the lowest value of all configurations tested, which indicates the effectiveness of its design concept. The low drag due to lift compensates for the high minimum drag of this configuration in determining its lift-drag ratio.

The arrow wing, however, has a drag due to lift which increases rapidly with Mach number and attains a maximum value of about 0.7 at M = 3. This value is about 40 percent greater than the theoretical estimate and corresponds in theory to that of a plane wing with supersonic leading edges such as for the delta-wing model.

[redacted]

The arrow-wing approach, however, is considered to have merit, for the design deficiencies of the initial model are now better understood and are capable of improvement. Although this configuration has attractive characteristics near $M = 3$, the optimum application may be found to occur at somewhat lower Mach numbers.

It should be noted that there are considerable additional wing-body data available at Mach numbers of about 3 which bear on the general problem of lift-drag ratio but which are not included herein. Although no positive statement can be made concerning their potential as to complete configurations, the drag-due-to-lift factors are, in general, less attractive than those of the complete configuration presented here.

Variation of Trim $\frac{L}{D}$ With $\frac{\partial C_m}{\partial C_L}$

Thus far mainly maximum lift-drag ratio characteristics of the various configurations have been considered. The cost of trimming over a range of stability margins is now considered. Figure 13 shows the variation in trim $\left(\frac{L}{D}\right)_{MAX}$ with stability level $\frac{\partial C_m}{\partial C_L}$ for values of test Mach number nearest 3. The curves were established from experimental data for which different control settings were used. For any of the configurations shown, trim at rather large stability margins can be obtained for rather small penalties in $\left(\frac{L}{D}\right)_{MAX}$. The trim $\left(\frac{L}{D}\right)_{MAX}$ for the canard model, however, begins to decrease at a somewhat lower stability margin than for the other models.

At the bottom of figure 13 are noted the supersonic stability margins required for neutral subsonic stability. These margins were determined from subsonic tests of the basic configurations and merely represent the shift of the aerodynamic center with Mach number. The plot shows that the experimental stability levels at $M \approx 3$ for the arrow-wing and outboard-tail models are higher than needed in order to maintain neutral subsonic stability. The particular canard configuration shown, however, would require an increase in supersonic stability level from the test conditions. Some performance penalty would result, therefore, unless special aerodynamic or mechanical methods are employed. The shift of the aerodynamic center shown is believed more a function of body-wing-inlet design rather than any inherent characteristic of the canard control. Canard models have been tested which have shown considerably less shift than that indicated here. (For example, see refs. 10 and 11.)

[redacted]

Figure 14 shows the predicted extrapolation to full-scale Reynolds numbers of the $\left(\frac{L}{D}\right)_{MAX}$ values for a Mach number of 3. A theoretical variation of skin friction with Reynolds number for adiabatic conditions (ref. 4) is assumed as well as the constancy of drag due to lift with Reynolds number. The experimental values of $\frac{L}{D}$ have been adjusted to $M = 3$ and are shown plotted at their respective test Reynolds numbers.

The dashed line is the theoretical extrapolation in lift-drag ratio starting from a mean test value of about 6 at a Reynolds number of 3 million. A ±10-percent spread from the theoretical turbulent skin-friction variation is also shown. This variation is indicative of the range from a small amount of laminar flow to all-turbulent flow with some roughness drag. Such an extrapolation presumes extreme care has been exercised in minimizing the drag due to roughness (ref. 12), protuberances, air leakage, and auxiliary inlets and outlets in order to justify limiting the model scale corrections to skin friction only. The problem of exit drag is discussed in reference 13.

The extrapolation is considered to provide evidence that values of $\left(\frac{L}{D}\right)_{MAX}$ of the order of 7.5 may be achieved at $M = 3$ for complete configurations at a Reynolds number of about 100 million. This value represents an attractive level of lift-drag ratio and results in a product of $M \times \frac{L}{D}$ for the basic range equation which exceeds the value for the best subsonic configurations.

An extrapolation of the lift coefficient at which $\left(\frac{L}{D}\right)_{MAX}$ occurs $\left(\text{that is, } C_{L,OPT}\right)$, when made on the basis of conditions identical with those used for $\left(\frac{L}{D}\right)_{MAX}$, shows that the full-scale values of $C_{L,OPT}$ would be expected to fall within the range from 0.09 to 0.11 for the configurations investigated.

CONCLUDING REMARKS

Results have been presented for essentially complete airplane configurations based on widely differing aerodynamic approaches to the problem of obtaining a high lift-drag ratio. Although the experimental programs were not sufficiently complete for an evaluation of the special features, high lift-drag ratios were obtained in all cases.

[redacted]

Maximum lift-drag ratios of about 6 were measured at a Mach number of 3 for test Reynolds number conditions. These values extrapolate to a maximum lift-drag ratio value on the order of 7.5 for full-scale Reynolds numbers of about 100 million.

The various configurations differed appreciably in minimum drag and in drag due to lift. There is reason to believe, therefore, that significant performance improvements can still be achieved, perhaps by combining some of the more attractive features of the different configurations.

Certain deficiencies noted for the various configurations, particularly with regard to trim and stability characteristics, do not appear to present problems prohibitive of solution.

Langley Aeronautical Laboratory,
National Advisory Committee for Aeronautics,
Langley Field, March 20, 1958.

[redacted]

REFERENCES

1. Katzen, Elliott D.: Idealized Wings and Wing-Bodies at a Mach Number of 3. NACA TN 4361, 1958.

2. Tucker, Warren A.: A Method for the Design of Sweptback Wings Warped to Produce Specified Flight Characteristics at Supersonic Speeds. NACA Rep. 1226, 1955. (Supersedes NACA RM L51F08.)

3. Grant, Frederick C.: The Proper Combination of Lift Loadings for Least Drag on a Supersonic Wing. NACA Rep. 1275, 1956. (Supersedes NACA TN 3533.)

4. Van Driest, E. R.: Turbulent Boundary Layer in Compressible Fluids. Jour. Aero. Sci., vol. 18, no. 3, Mar. 1951, pp. 145-160, 216.

5. Hallissy, Joseph M., Jr., and Hasson, Dennis F.: Aerodynamic Characteristics at Mach Numbers 2.36 and 2.87 of an Airplane Configuration Having a Cambered Arrow Wing With a 75° Swept Leading Edge. NACA RM L58E21, 1958.

6. Sleeman, William C., Jr.: Preliminary Study of Airplane Configurations Having Tail Surfaces Outboard of the Wing Tips. NACA RM L58B06, 1958.

7. Church, James D., Hayes, William C., Jr., and Sleeman, William C., Jr.: Investigation of Aerodynamic Characteristics of an Airplane Configuration Having Tail Surfaces Outboard of the Wing Tips at Mach Numbers of 2.30, 2.97, and 3.51. NACA RM L58C25, 1958.

8. Kelly, Thomas C., Carmel, Melvin M., and Gregory, Donald T.: An Exploratory Investigation at Mach Numbers of 2.50 and 2.87 of a Canard Bomber-Type Configuration Designed for Supersonic Cruise Flight. NACA RM L58B28, 1958.

9. Mueller, James N.: An Investigation of the Effect of Varying the Maximum-Thickness Position Upon the Aerodynamic Characteristics of a Series of $3\frac{1}{2}$-Percent-Thick Delta Wings. NACA RM L55D26, 1955.

10. Spearman, M. Leroy, and Driver, Cornelius: Some Factors Affecting the Stability and Performance Characteristics of Canard Aircraft Configurations. NACA RM L58D16, 1958.

11. Hall, Charles F., and Boyd, John W.: Effects of Canards on Airplane Performance and Stability. NACA RM A58D24, 1958.

[redacted]

12. Czarnecki, K. R., Sevier, John R., Jr., and Carmel, Melvin M.: Effects of Fabrication-Type Roughness on Turbulent Skin Friction at Supersonic Speeds. NACA TN 4299, 1958.

13. Swihart, John M., and Nelson, William J.: Performance of Multiple Jet-Exit Installations. NACA RM L58E01, 1958.

[redacted]

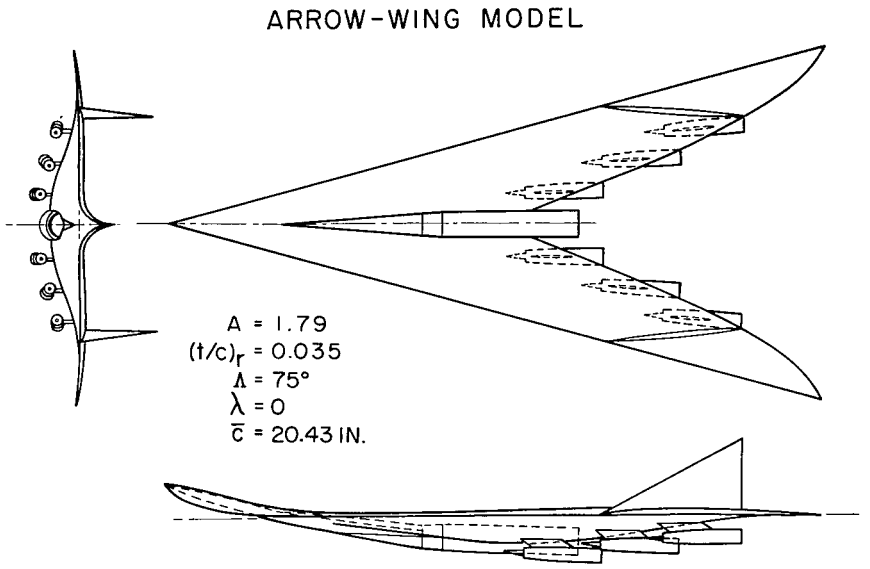

Figure 1

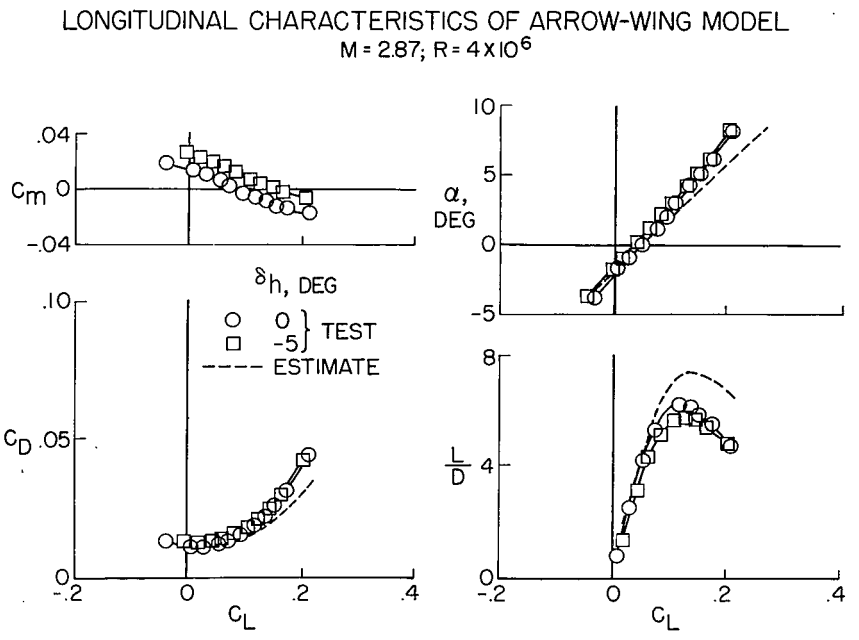

Figure 2

[redacted]

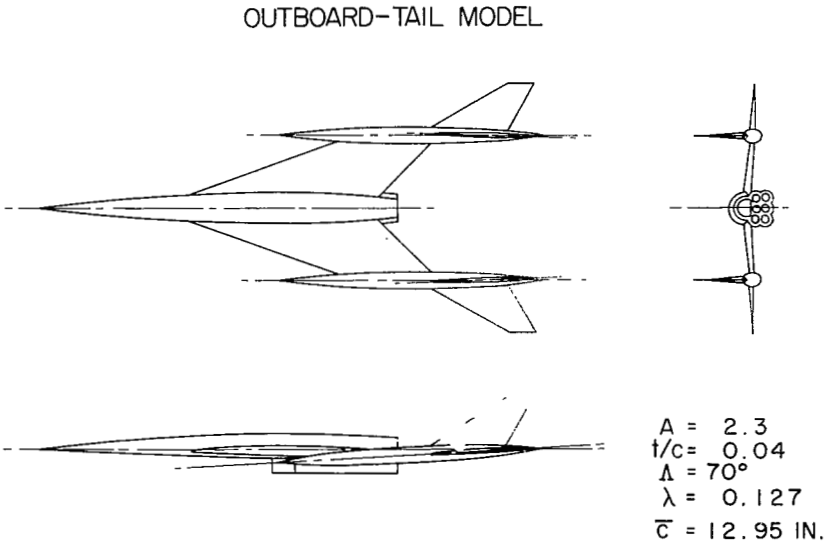

Figure 3

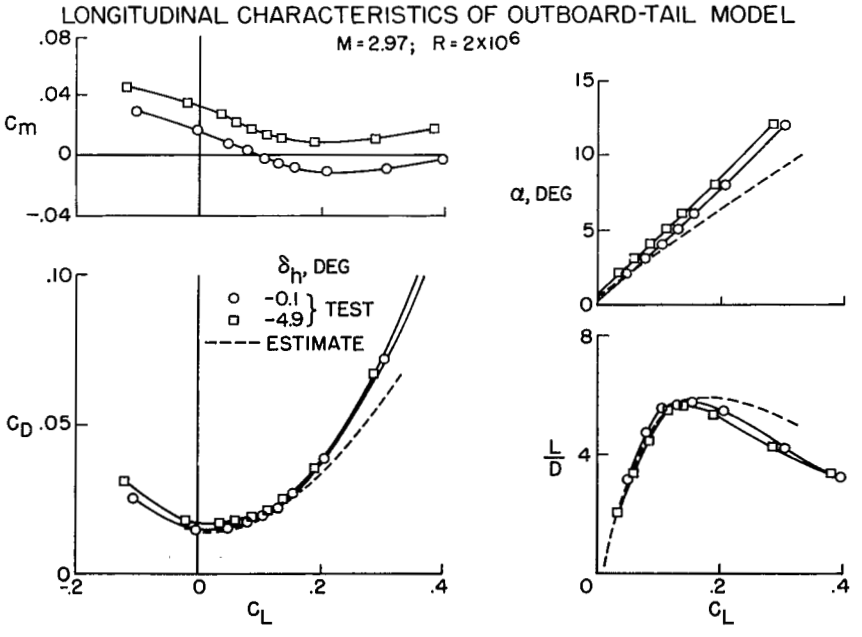

Figure 4

[redacted]

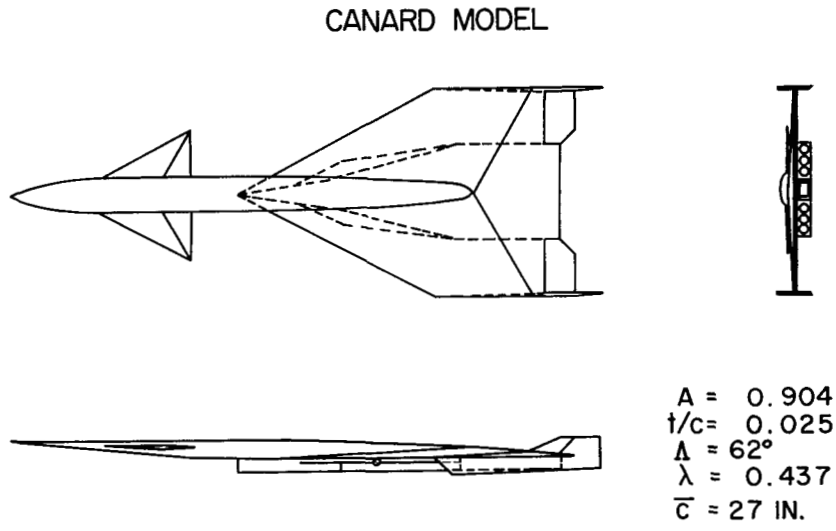

Figure 5

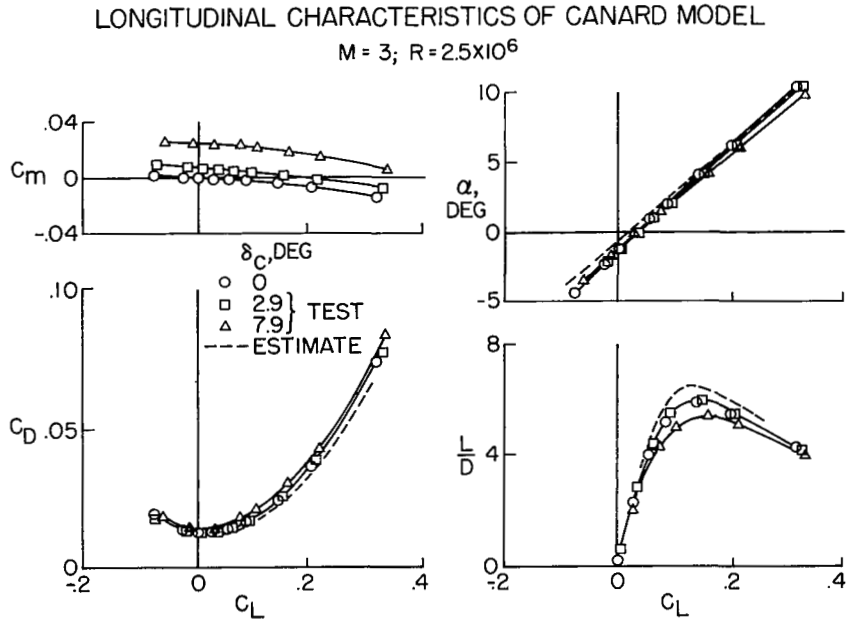

Figure 6

[redacted]

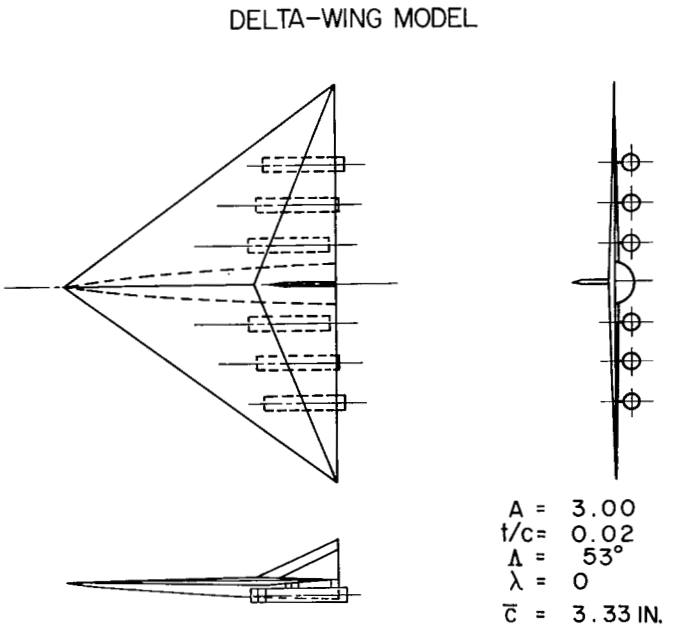

Figure 7

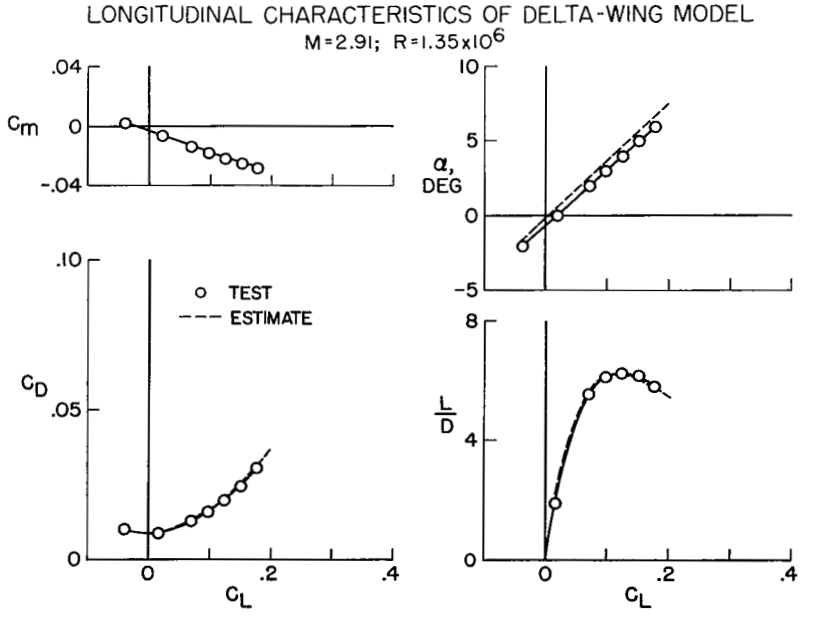

Figure 8

[redacted]

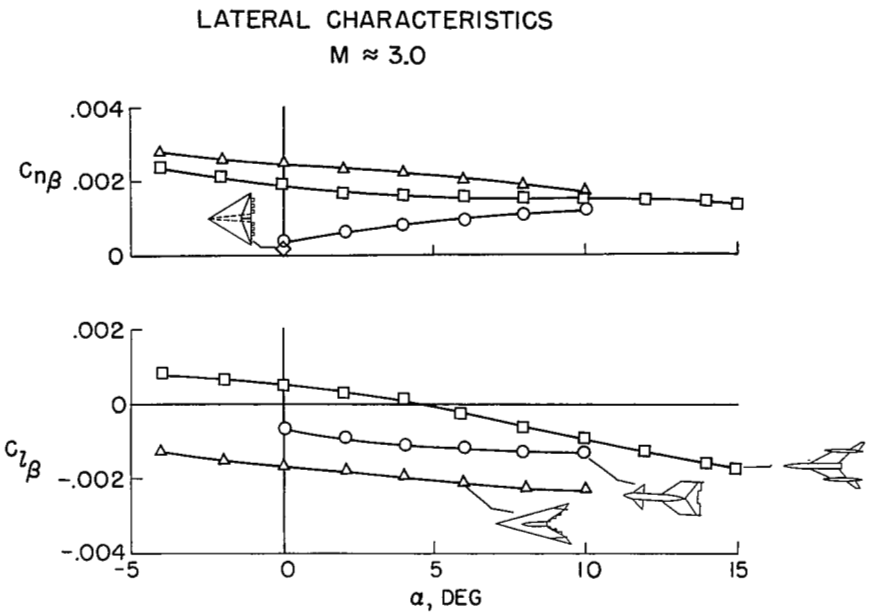

Figure 9

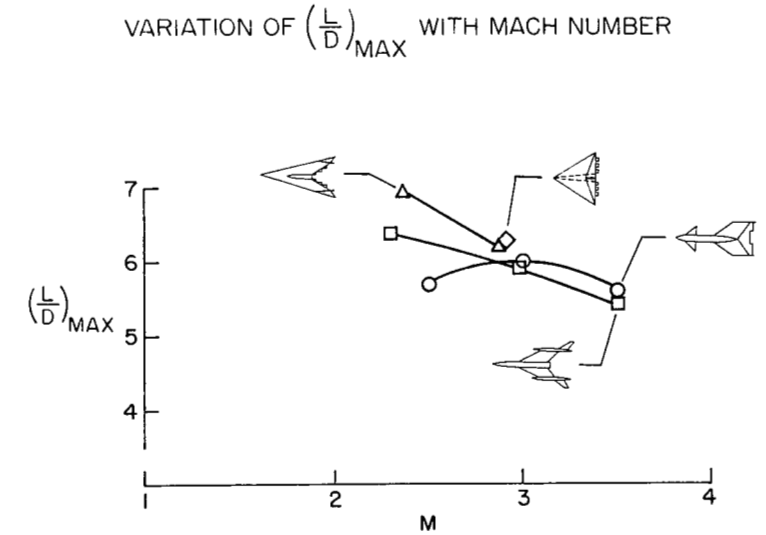

Figure 10

[redacted]

DRAG POLAR ANALYSIS

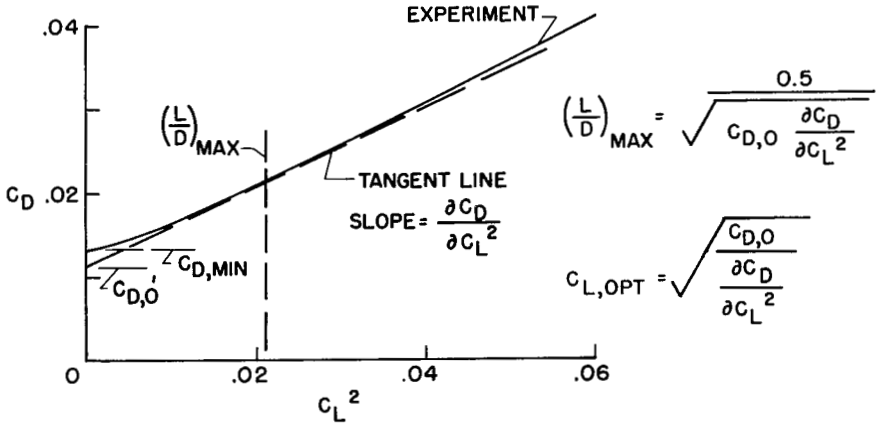

Figure 11

VARIATIONS OF $C_{D,MIN}$ AND $\frac{\partial C_D}{\partial C_L^2}$ WITH MACH NUMBER

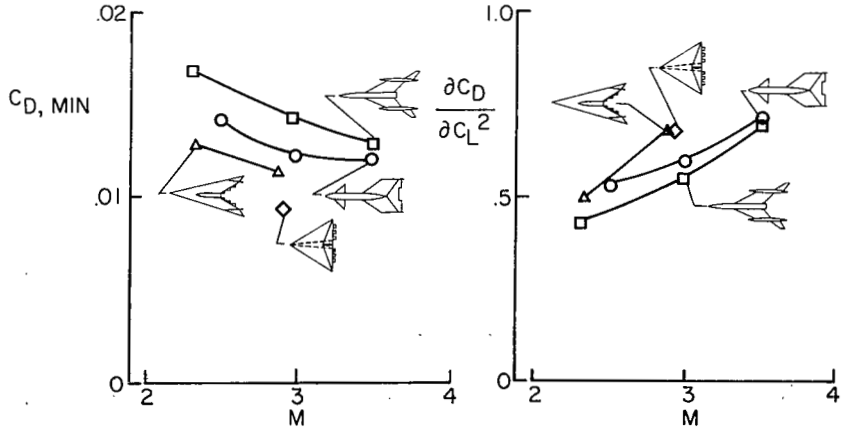

Figure 12

[redacted]

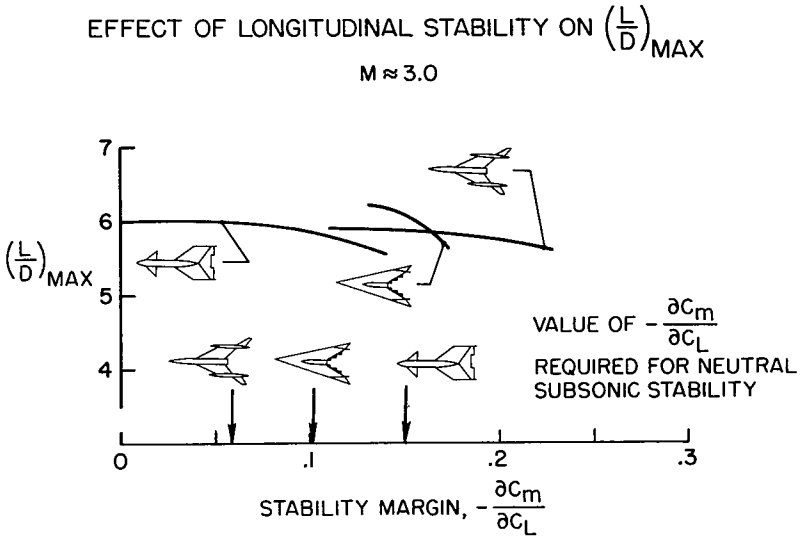

Figure 13

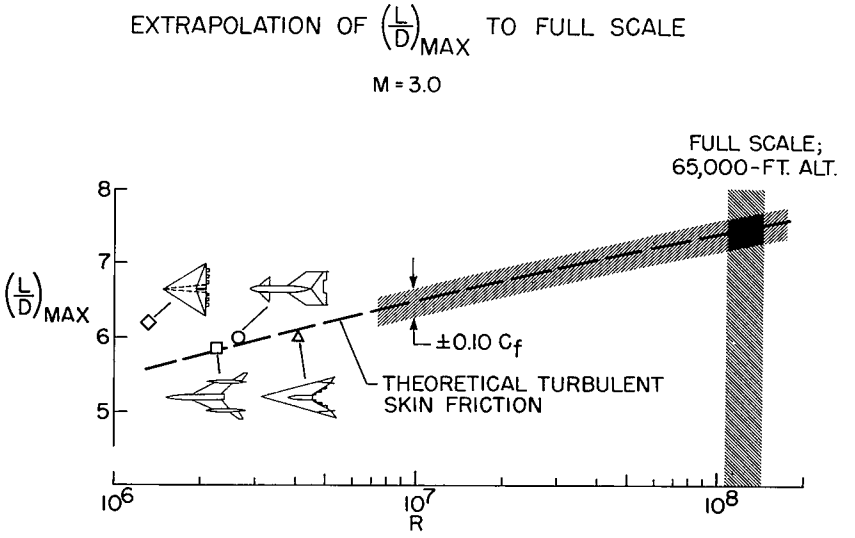

Figure 14

[redacted]